Brief Communication: Drought Likelihood for East Africa

Hui Yang[1, 2], Chris Huntingford[2]

[1]Department of Ecology, School of Urban and Environmental Sciences, Peking University, Beijing, P. R. China
[2]Centre for Ecology and Hydrology, Wallingford, Oxfordshire, OX10 8BB, U.K.

5   *Correspondence to*: Hui Yang (yang_hui@pku.edu.cn)

Abstract. East Africa autumn drought in 2016 caused malnutrition, illness and death. Close to 16 million people across Somalia, Ethiopia and Kenya needed food, water and medical assistance. Many factors influence drought stress and response. However, inevitably it is asked: are elevated greenhouse gas concentrations altering extreme rainfall deficit frequency? We investigate with General Circulation Model (GCMs). After bias correction to match contemporary rainfall

10   mean, GCMs project small decreases in probability of drought of same severity for East Africa by the end of 21st century. However, further adjusting the variance of GCMs to match ERA-interim data, probability of drought increases slightly.

ECMWF re-analysis data (ERA-interim; Dee et al., 2011) shows that during August to October (ASO) of 2016, large parts of Somalia, Ethiopia and Kenya (Black rectangle, Fig. 1a) had a reduction of 30% or more in rainfall compared to a baseline

15   ASO period 1979-2015. For this region, the spatial average of monthly rainfall during ASO of 2016 lies at least one standard deviation below the climatological mean of the other years (Fig. 1b). The year of 2016 is the third driest year in the past four decades. Other years with rainfall at least on standard deviation below the climatological mean during 1979-2015 are 1986, 1990,1991, 1993 and 2010. Year of 2010 also suffered from the severe famine (Dutra et al., 2013). We concentrate on East Africa, as this region experienced particularly poor harvest and where famine was widely reported during 2016 (noting that

20   regions outside black rectangle of Fig. 1a also experienced major rainfall deficits in 2016). East Africa is especially vulnerable to the impacts of drought (DEC, 2017). The region has long experienced widespread poverty and high levels of food insecurity (Von Grebmer et al., 2016). The high dependence of its population on rain-fed agriculture, sometimes in tandem with political instability, exacerbate the impacts of droughts (Love, 2009; Masih et al., 2014).

25   To assess any influence of increasing atmospheric GHG concentrations, we use monthly rainfall data from 37 GCMs simulations for the historical period and for a high emission future scenario RCP8.5. These are from the Coupled Model Intercomparison Project Phase 5 (CMIP5, Taylor et al., 2012). A summary of the main characteristics of the models are provided in Table S1. A bias correction with two post-processing steps is applied to the GCM precipitation estimates. We first calculate modelled and ERA-based mean ASO rainfall estimates over the east Africa during the period 1979-2015. The

30   GCM precipitation estimates, both past and future, are corrected by a GCM-specific mean correction factor, which is a ratio of the climatological mean of each GCM to that of the ERA-interim reanalysis product. Second, we then adjust the

climatological standard deviation (STD) of GCM precipitation estimates by multiplying the ratio of the climatological STD of each GCM to that of the ERA-interim data. The adjustment of spread of rainfall distribution is an important additional procedure to further constrain GCM estimates (Sippel et al., 2016; Jeon et al., 2016; Angelil et al., 2017). Together this ensures all GCMs have the ERA-based mean and STD for period 1979-2015. Each GCM is considered equally plausible. Bias-corrected mean ASO rainfall are presented in Fig. 1c for mean bias correction, and in Fig. 1d for mean and STD bias correction. These are derived from 37 GCMs, and for four 31-year periods (pre-industrial, present day, and two future periods).

We estimate the probability, in any year, of rainfall being less than 46 mm per month. This threshold is 35% less than the climatological ASO mean, and is the ASO mean rainfall level in 2016 (red curve within yellow highlight, Fig. 1b). For the mean-corrected GCM estimates, we compare (inset, Fig. 1c) modelled period 1861-1891, representative of pre-industrial, with present day (period 2001-2031), and find this probability decreases slightly from 3.8% (STD ± 0.5%) to 2.8% (STD ± 0.5%). The one standard deviations are estimated via bootstrapping with 80% replications from the 37 GCM precipitation data and for the 31-year periods. These trends continue, giving probabilities 2.3% (± 0.5%) and 2.1% (± 0.4%) for periods 2035-2065 and 2070-2100 respectively. For the mean- and variance-corrected GCM estimates (Fig. 1d), we found the probability of east African drought is smallest at present (0.4% ± 0.2%, period 2001-2031). Such probability would become larger in the future, giving probabilities 1.1% (± 0.4%) and 1.2% (± 0.3%) for periods 2035-2065 and 2070-2100 respectively. Hence we find accounting for model biases in the variance of GCM distributions has the potential to significantly alter the predictions of drought events occurrence over the east Africa.

Given that large uncertainty in the observation-based precipitation products has been well reported (Angélil et al., 2016), we use four other precipitation estimates (GPCP, PREC/L, CPC and TRMM) to bias-correct GCM estimates. In Fig. 2 we reproduce the insets of Fig 1c (no hatching) and Fig 1d (hatching) for ERA-Interim, and then for the four other precipitation products. Consistent with the conclusions based on the ERA-interim product only, the results from the other rainfall products also show that the probability of drought occurrence in the east Africa has decreased slightly from pre-industrial to present day, and irrespective of whether variance adjustment has occurred (Fig. 2, all blue and black bars, with and without hatching). Future projections, though, of drought likelihood do vary across different precipitation products. For the mean-corrected GCM estimates, 4 out of 5 rainfall product-corrected GCM projections give a slight decrease in drought occurrence likelihoods by the end of 21st century. The exception is the TRMM-corrected GCMs, which suggest the drought probability would increase slightly by 2070-2100 and relative to the present day. For the mean- and variance-corrected GCM estimates, relative to the present-day levels the GCM estimates corrected to the ERA-interim, GPCP, and TRMM products give an increase in drought occurrence probability. However PREC/L- and CPC-corrected GCM estimates suggest the probability of drought occurrence will decrease. This divergence is due to the strong differences in the climatological mean, standard deviation and year 2016 ASO rainfall levels among the different precipitation products (Table S2).

The multi-model ensemble forecast, corrected by the ERA-interim rainfall product and merging the individual forecasts with equal weights, shows that the east African mean ASO rainfall for 2070-2100 will increase significantly, compared with the present period 2001-2031 (main PDFs, Fig 1c.,d.). It is these general increases that even in conjunction with larger future distribution spreads, imply no significant increase of drought occurrence probability (Fig 1c., d.). In Fig. 3, we present for the individual models, changes in numbers of years of mean ASO rainfall falling below 46 mm per month. We also show individual model changes in mean and STD of ASO rainfall, for 31 years 2070-2100 compared to 2001-2031. Fig. 3 shows 28 out of 37 model estimates for this region become wetter, and most models (i.e. 22 out of 37 models) exhibiting increased distribution spreads reflected by raised STDs. Models generally agree on the direction of these changes, but the magnitude of changes in GCMs remains uncertain.

Our analysis reveals that current understanding of how future climate change will impact on East Africa ASO drought risk remains uncertain. This is based on a relatively simple assessment of 37 climate models, each given equal weight but after being corrected by observation-based rainfall products. We find the sources of uncertainty in drought prediction include: 1) the choice of bias correction methodology; 2) the choice of observational product used to correct bias in GCMs; and 3) the choice of GCMs used. Currently, for many geographical regions, GCM estimates of rainfall changes varies substantially across models (Knutti and Sedláček, 2013). Multi-model analyses such as ours consider uncertainty associated with different model parameterisation or scheme describing rainfall features. However, to give more definitive answers, the climate research community may need to be confident enough to rank climate models based on performance to refine future projections (Knutti et al., 2017). Improving GCM projections also could involve on-going constraining of model components. For rainfall of east Africa predictions in particular, this will link to accurate forward projections of oceanic variability. Strong teleconnections are known to exist between El Niño Southern Oscillation (ENSO) and East African rainfall (Segele et al., 2009; Gissila et al., 2004), and with longer-term fluctuations in Pacific SSTs increasing/decreasing rainfall (Funk et al., 2014; Liebmann et al., 2014). Larger ensembles of simulations by each model is also important, and especially when analysing the probability of extreme events. This enables a more complete sampling of probability distributions, describing more fully the internal variability of the climate system imposed over general climate change. In addition, some GCMs estimate an increase in future variability of east African ASO rainfall, and better knowledge of the magnitude of this is important. Research shows any variability increases as well as mean changes has strong impacts on society (Brown and Lall, 2006). Furthermore, food and water availability in East Africa has multiple socio-economic drivers, alongside climatic influences (Little et al., 2001; Adhikari et al., 2015). Although here we have focused on climate model projections of the future, more holistic approaches will combine climate and crop impact modelling. The hope is that climate model predictions for east Africa will move towards a consensus on expected changes, helping then better protection and disaster preparedness against future famine.

References

Adhikari, U., Nejadhashemi, A.P., and Woznicki, S.A., 2015. Climate change and Eastern Africa: A review of impact on Major Crops. Food Energy Secur. 4(2), 110-132.

Angélil, O., Perkins-Kirkpatrick, S., Alexander, L.V., Stone, D., Donat, M.G., Wehner, M., Shiogama, H., Ciavarella, A. and Christidis, N., 2016. Comparing regional precipitation and temperature extremes in climate model and reanalysis products. Weather Clim. Extremes, 13, 35-43.

Brown, C. and Lall, U., 2006. Water and economic development: The role of variability and a framework for resilience. In *Natural Resources Forum* (Vol. 30, No. 4, pp. 306-317). Blackwell Publishing Ltd.

DEC, 2017. Disasters Emergency Committee; https://www.dec.org.uk/splash/africa.

Dee, D.P., Uppala, S.M., Simmons, A.J., Berrisford, P., Poli, P., Kobayashi, S., Andrae, U., Balmaseda, M.A., Balsamo, G., Bauer, P. and Bechtold, P., 2011. The ERA-Interim reanalysis: configuration and performance of the data assimilation system, Q. J. R. Meteorolog. Soc., 137, 553-597.

Dutra, E., Magnusson, L., Wetterhall, F., Cloke, H.L., Balsamo, G., Boussetta, S. and Pappenberger, F., 2013. The 2010-2011 drought in the Horn of Africa in ECMWF reanalysis and seasonal forecast products. Int. J. Climatol., 33(7), 1720-1729.

Funk, C., Hoell, A., Shukla, S., Blade, I., Liebmann, B., Roberts, J.B., Robertson, F.R. and Husak, G., 2014. Predicting East African spring droughts using Pacific and Indian Ocean sea surface temperature indices. Hydrol. Earth Syst. Sci., 18(12), 4965-4978.

Gissila, T., Black, E., Grimes, D.I.F. and Slingo, J.M., 2004. Seasonal forecasting of the Ethiopian summer rains. Int. J. Climatol., 24(11), 1345-1358.

Masih, I., Maskey, S., Mussá, F.E.F. and Trambauer, P., 2014. A review of droughts on the African continent: a geospatial and long-term perspective. Hydrol. Earth Syst. Sci., 18(9), 3635.

Jeon, S., Paciorek, C.J. and Wehner, M.F., 2016. Quantile-based bias correction and uncertainty quantification of extreme event attribution statements. Weather Clim. Extremes, 12, 24-32.

Knutti, R. and Sedláček, J., 2013. Robustness and uncertainties in the new CMIP5 climate model projections. Nat. Clim. Change, 3(4), 369-373.

Knutti, R., Sedláček, J., Sanderson, B.M., Lorenz, R., Fischer, E.M. and Eyring, V., 2017. A climate model projection weighting scheme accounting for performance and interdependence. Geophys. Res. Lett., 44(4), 1909-1918.

Little, P.D., Smith, K., Cellarius, B.A., Coppock, D.L. and Barrett, C., 2001. Avoiding disaster: diversification and risk management among East African herders. Dev. Change., 32(3), 401-433.

Love, R., 2009. Economic Drivers of Conflict and Cooperation in the Horn of Africa. Chatham House Briefing Paper, December. Available at: www. chathamhouse. org/publications/papers/view/109208 (accessed 18 April 2012).

Segele, Z.T., Lamb, P.J. and Leslie, L.M., 2009. Large-scale atmospheric circulation and global sea surface temperature associations with Horn of Africa June–September rainfall. Int. J. Climatol., 29(8), 1075-1100.

Sippel, S., Otto, F.E.L., Forkel, M., Allen, M.R., Guillod, B.P., Heimann, M., Reichstein, M., Seneviratne, S.I., Thonicke, K. and Mahecha, M.D., 2016. A novel bias correction methodology for climate impact simulations. Earth Syst. Dyn., 7(1), 71-88.

Taylor, K.E., Stouffer, R.J. and Meehl, G.A., 2012. An overview of CMIP5 and the experiment design. Bull. Am. Meteorol. Soc., 93(4), 485-498.

Von Grebmer, K., Bernstein, J., Nabarro, D., Prasai, N., Amin, S., Yohannes, Y., Sonntag, A., Patterson, F., Towey, O. and Thompson, J., 2016. 2016 Global hunger index: Getting to zero hunger. Intl Food Policy Res Inst.

Yang, W., Seager, R., Cane, M.A. and Lyon, B., 2014. The East African long rains in observations and models. . J. Clim., 27(19), 7185-7202.

Acknowledgements

HY gratefully acknowledges funding from the China Scholarship Council, and CH acknowledges the NERC CEH Science Budget. The authors acknowledge the World Climate Research Programme's Working Group on Coupled Modelling, which

15

is responsible for CMIP, and we thank the climate modelling groups for producing and making available their model output. We also acknowledge the re-analysis products of the European Centre for Medium-Range Weather Forecasts.

Rainfall for Aug to Oct, 2016 as a percent change from the average (%)
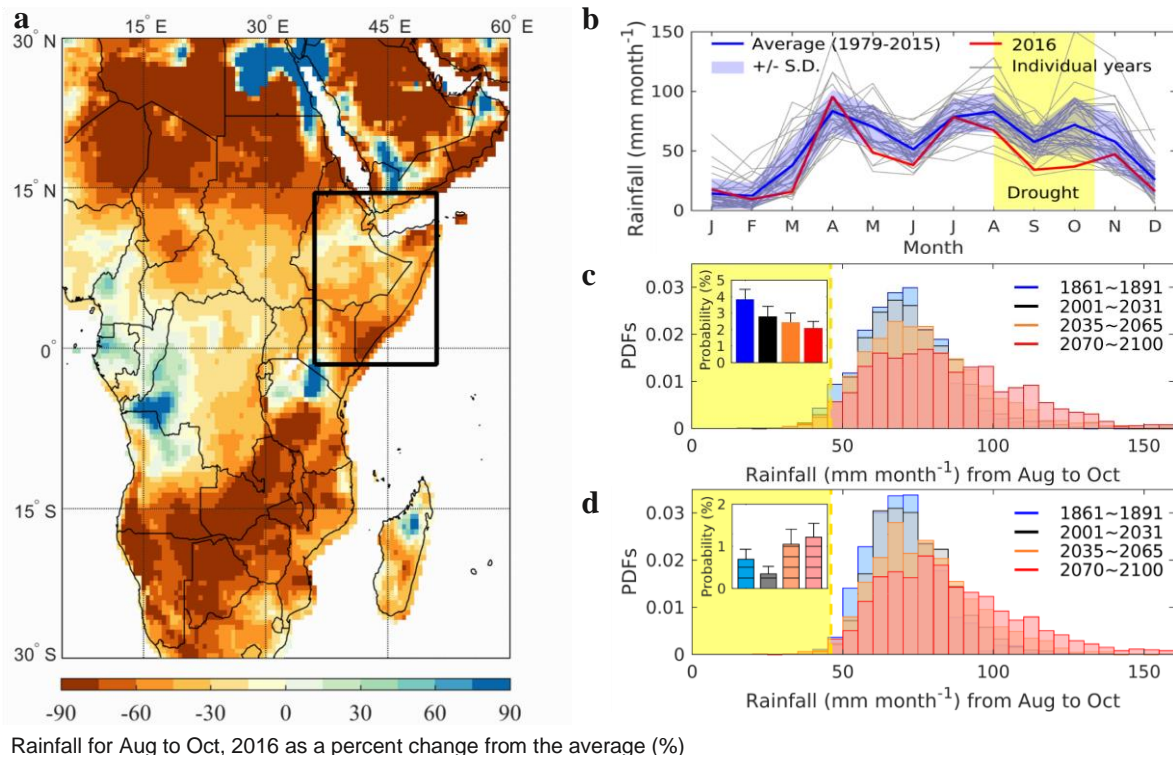
Figure 1: (**a**) Black rectangle is location of study region (14.5°N~1.5°S, 36°E~51°E). Plotted is mean rainfall for 2016 and months August to October inclusive (ASO), presented relative changes (as %) to long-term average ASO values (1979-2015). Values based on ERA-interim reanalysis product. (**b**) ERA-based monthly total rainfall (mm month^{-1}) over study region (panel a; land within black rectangle) for years 1979 to 2016. Year 2016 is red, other years are individual grey lines, and multi-year average (not including 2016) is blue line. Blue shading is ± one standard deviation of monthly rainfall across years 1979-2015. The drought event (shaded in yellow) is defined as the three consecutive months of ASO, and when rainfall in year 2016 is below blue shading. (**c**) CMIP5-based PDFs of mean ASO rainfall for periods 1861-1891 (blue), 2001-2031 (black), 2035-2065 (orange) and 2070-2100 (red). Each curve corresponds to the mean-corrected combined outputs from 37 CMIP5 models forced by historical emissions and RCP8.5 future scenario. Individual GCM bias correction is based on the ERA-interim reanalysis product. Yellow shading is mean ASO rainfall less than 46 mm month^{-1}, which is the ERA-interim 2016-based threshold (mean of ASO, red curve in panel b). Inset shows probabilities of mean rainfall of ASO falling below the threshold for the same modelled periods (colours match those of curves). The error bars are the standard deviations (estimated via bootstrapping 80% replications from the 37 GCM precipitation data for the 31-year periods). (**d**) same as (**c**), but based on the mean- and variance-corrected GCM rainfall estimates.
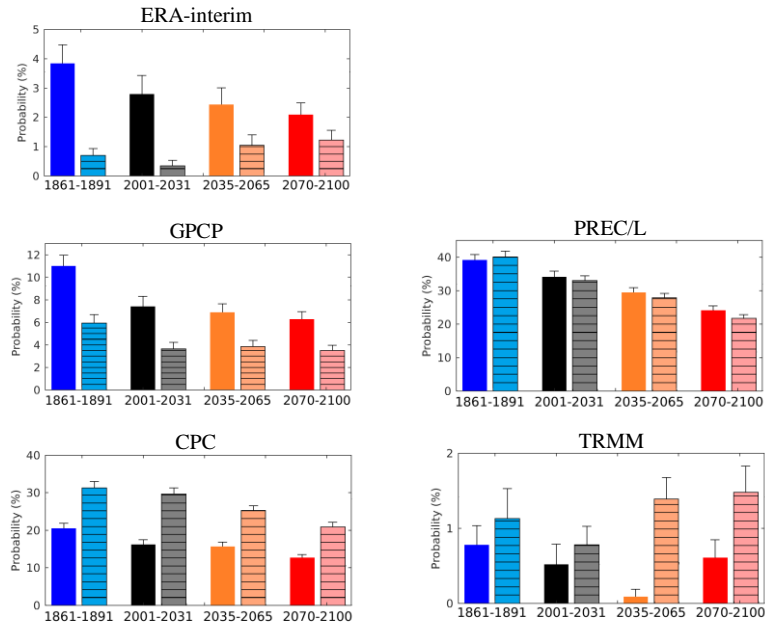
Figure 2: CMIP5-based histograms of probabilities of mean ASO rainfall falling below year 2016-based threshold values. Shown for periods 1861-1891 (blue), 2001-2031 (black), 2035-2065 (orange) and 2070-2100 (red). Each bar corresponds to merged normalized outputs from 37 CMIP5 models forced by historical emissions and RCP8.5 future scenario. The bars without horizontal hatching (left) are for the mean-corrected GCM precipitation estimates. The bars with hatching (right) are for the mean- and variance-corrected GCM estimates.
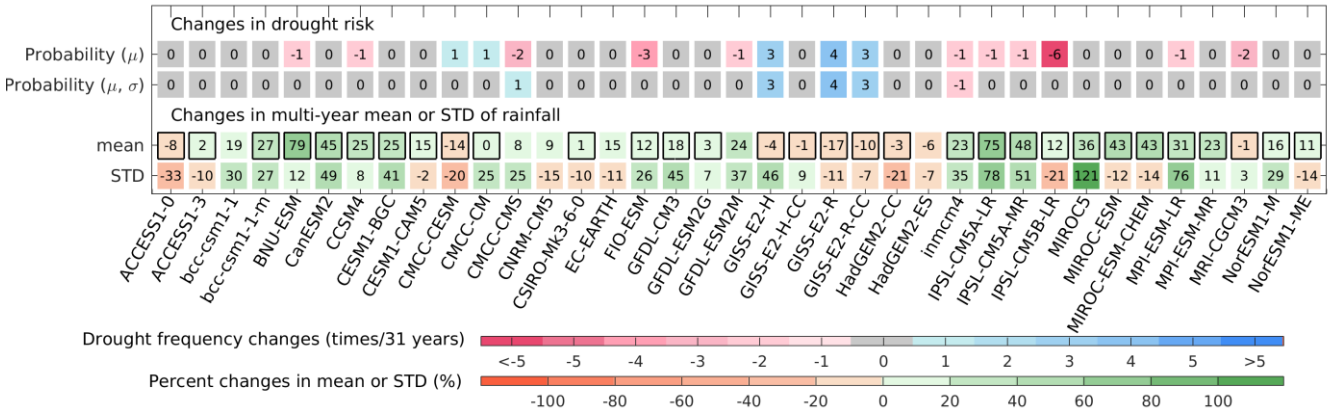
Figure 3: Changes in drought frequency, multi-year mean and standard deviations (STD) of 31 consecutive year rainfall amounts. Difference between present period 2001-2031 and period 2070-2100, as estimated by 37 GCMs. GCM estimates are corrected by the ERA-interim rainfall product. Changes to frequencies of drought occurrence are estimated from the mean bias-corrected GCM estimates (1st row), both mean- and variance bias-corrected GCM estimates (2nd row). The colored grids in the 3rd row with black borders indicate statistically significant differences in the 31-year rainfall mean between these two periods (t-test, with $P < 0.05$). The percentage changes are calculated as $[(x_{2070-2100}/x_{2001-2031})-1] \times 100\%$.

Supplementary Information

Table S1. CMIP5 global circulation models (GCMs) used in this study, and their components.

Model Name	Atmospheric Model	Land surface Model	Oceanic Model	Reference
ACCESS1-0	HadGEM2 r1.1	MOSES	MOM4pl	*Bi et al.*(2012)
ACCESS1-3	Similar to GA 1.0	CABLE v1.8	MOM4p	
bcc-csm1-1	BCC_AGCM2.2	BCC_AVIM1.0	MOM4_L40	*Wu et al.* (2012)
bcc-csm1-1-m	BCC_AGCM2.2	BCC_AVIM1.0	MOM4_L40	
BNU-ESM	CAM3.5	CLM	MOM4p1	*Ji et al.* (2014)
CanESM2	CanAM4	CLASS2.7	CanOM4 and CMOC1.2	*Arora et al.* (2011)
CCSM4	CAM4	CLM4	POP2	*Gent et al.* (2011)
CESM1-BGC	CAM4	CLM4	POP2	*Neale et al.* (2010)
CESM1-CAM5	CAM5	CLM4	POP2	
CMCC-CESM	ECHAM5	SILVA	NEMO	*Scoccimarro et al.* (2011)
CMCC-CM	ECHAM5	SILVA	OPA 8.2	
CMCC-CMS	ECHAM5	SILVA	OPA 8.2	
CNRM-CM5	ARPEGE climate	SURPEXv5.1	NEMO3.3	*Voldoire et al.* (2011)
CSIRO-Mk3-6-0	AGCMv7.3.8	a soil-canopy scheme	GFDL MOM2.2	*Rotstayn et al.* (2010)
EC-EARTH	IFS	H-TESSEL	NEMO	Hazeleger et al. (2010)
GFDL-CM3	GFDL-AM3	LM3	MOM	*Griffies et al.* (2011)
GFDL-ESM2G	GFDL-AM2.1	LM3	GOLD	*Dunne et al.* (2012)
GFDL-ESM2M	GFDL-AM2.1	LM3	MOM4	
GISS-E2-H-CC	GISS-E2	GISS-LSM-CC	HYCOM	*Schmidt et al.* (2014)
GISS-E2-H	GISS-E2	GISS-LSM	HYCOM	
GISS-E2-R-CC	GISS-E2	GISS-LSM-CC	Russell	
GISS-E2-R	GISS-E2	GISS-LSM	Russell	
HadGEM2-CC	HadGAM2	TRIFFID	HadGOM2	*Collins et al.* (2011)
HadGEM2-ES	HadGAM2	TRIFFID	HadGOM2	*Jones et al.* (2011)
INMCM4	INM	INM	HadGOM2	*Volodin et al.* (2010)
IPSL-CM5A-LR	LMDZ5A	ORCHIDEE	NEMO	*Dufresne et al.* (2012)
IPSL-CM5A-MR	LMDZ5A	ORCHIDEE	NEMO	
IPSL-CM5B-LR	LMDZ5B	ORCHIDEE	NEMO	
MIROC5	FRCGC-AGCM	MATSIRO	COCO4.5	*Watanabe et al.* (2011)
MIROC-ESM	FRCGC-AGCM	MATSIRO	COCO4.5	
MIROC-ESM-CHEM	FRCGC-AGCM	MATSIRO	COCO4.5	
MPI-ESM-LR	ECHAM6	JSBACH	MPIOM	*Ilyina et al.* (2013)
MPI-ESM-MR	ECHAM6	JSBACH	MPIOM	
MRI-CGCM3	MRIÕAGCM3	HAL	MRI.COM3	*Yukimoto et al.* (2012)
NorESM1-ME	CAM4-Oslo	CLM4	MICOM	*Tjiputra et al.* (2013)
NorESM1-M	CAM4-Oslo	CLM4	MICOM	

Table S2. The mean August-to-October (ASO) rainfall (mm month^{-1}) of year 2016, multi-year mean (not including 2016) and multi-year standard deviation (STD) over east Africa for years 1979 to 2016. The five global precipitation data sets used are listed. Four products of ERA-interim, GPCP, PREC/L, CPC and TRMM are available from 1979 to 2016. These four precipitation data sets are either interpolated gauge observations only (i.e. PREC/L and CPC), gauge observations combined with satellite measurements (i.e. GPCP), or reanalysis data (i.e. ERA-interim). The TRMM satellite observations are available from 2001 to 2016.

ASO rainfall (mm month^{-1})	ERA-interim	GPCP	PREC/L	CPC	TRMM
2016	46.10	46.56	57.16	35.78	32.05
Climatological mean (1979-2015)	70.76	62.78	61.68	43.44	60.69*
Climatological STD (1979-2015)	11.28	10.40	11.48	13.89	11.83*

* TRMM satellite precipitation data is only available from 2001 to 2016. The climatological ASO rainfall averages of the period 2001-2015 is computed.

References

Arora, V.K., Scinocca, J.F., Boer, G.J., Christian, J.R., Denman, K.L., Flato, G.M., Kharin, V.V., Lee, W.G. and Merryfield, W.J., 2011. Carbon emission limits required to satisfy future representative concentration pathways of greenhouse gases. Geophys. Res. Lett., 38(5).

Bi, D., Dix, M., Marsland, S.J., O'Farrell, S., Rashid, H., Uotila, P., Hirst, A., Kowalczyk, E., Golebiewski, M., Sullivan, A. and Yan, H., 2013. The ACCESS coupled model: description, control climate and evaluation. Aust. Meteorol. Oceanogr. J, 63(1), 41-64.

Collins, W.J., Bellouin, N., Doutriaux-Boucher, M., Gedney, N., Halloran, P., Hinton, T., Hughes, J., Jones, C.D., Joshi, M., Liddicoat, S. and Martin, G., 2011. Development and evaluation of an Earth-System model-HadGEM2. Geosci. Model Dev., 4(4), 1051.

Dufresne, J.L., Foujols, M.A., Denvil, S., Caubel, A., Marti, O., Aumont, O., Balkanski, Y., Bekki, S., Bellenger, H., Benshila, R. and Bony, S., 2013. Climate change projections using the IPSL-CM5 Earth System Model: from CMIP3 to CMIP5. Clim. Dyn., 40(9-10), 2123-2165.

Dunne, J.P., John, J.G., Adcroft, A.J., Griffies, S.M., Hallberg, R.W., Shevliakova, E., Stouffer, R.J., Cooke, W., Dunne, K.A., Harrison, M.J. and Krasting, J.P., 2012. GFDL's ESM2 global coupled climate–carbon earth system models. Part I: Physical formulation and baseline simulation characteristics. J. Clim., 25(19), 6646-6665.

Gent, P.R., Danabasoglu, G., Donner, L.J., Holland, M.M., Hunke, E.C., Jayne, S.R., Lawrence, D.M., Neale, R.B., Rasch, P.J., Vertenstein, M. and Worley, P.H., 2011. The community climate system model version 4. J. Clim., 24(19), 4973-4991.

Griffies, S.M., Winton, M., Donner, L.J., Horowitz, L.W., Downes, S.M., Farneti, R., Gnanadesikan, A., Hurlin, W.J., Lee, H.C., Liang, Z. and Palter, J.B., 2011. The GFDL CM3 coupled climate model: characteristics of the ocean and sea ice simulations. J. Clim., 24(13), 3520-3544.

Hazeleger, W., Severijns, C., Semmler, T., Ştefănescu, S., Yang, S., Wang, X., Wyser, K., Dutra, E., Baldasano, J.M., Bintanja, R. and Bougeault, P., 2010. EC-Earth: a seamless earth-system prediction approach in action. Bull. Am. Meteorol. Soc., 91(10), 1357-1363.

Ilyina, T., Six, K.D., Segschneider, J., Maier-Reimer, E., Li, H. and Núñez-Riboni, I., 2013. Global ocean biogeochemistry model HAMOCC: Model architecture and performance as component of the MPI-Earth system model in different CMIP5 experimental realizations. J. Adv. Model. Earth Syst., 5(2), 287-315.

Ji, D., Wang, L., Feng, J., Wu, Q., Cheng, H., Zhang, Q., Yang, J., Dong, W., Dai, Y., Gong, D. and Zhang, R.H., 2014. Description and basic evaluation of Beijing Normal University Earth system model (BNU-ESM) version 1. Geosci. Model Dev., 7(5), 2039-2064.

Jones, C., Hughes, J.K., Bellouin, N., Hardiman, S.C., Jones, G.S., Knight, J., Liddicoat, S., O'Connor, F.M., Andres, R.J., Bell, C. and Boo, K.O., 2011. The HadGEM2-ES implementation of CMIP5 centennial simulations. Geosci. Model Dev., 4(3), 543.

Neale, R. B., and Coauthors, 2010: Description of the NCAR Community Atmosphere Model (CAM5.0). NCAR Tech. Rep. NCAR/TN-4861STR, 268 pp.

Rotstayn, L.D., Jeffrey, S.J., Collier, M.A., Dravitzki, S.M., Hirst, A.C., Syktus, J.I. and Wong, K.K., 2012. Aerosol-and greenhouse gas-induced changes in summer rainfall and circulation in the Australasian region: a study using single-forcing climate simulations. Atmos. Chem. Phys., 12(14), 6377.

Schmidt, G.A., Ruedy, R., Hansen, J.E., Aleinov, I., Bell, N., Bauer, M., Bauer, S., Cairns, B., Canuto, V., Cheng, Y. and Del Genio, A., 2006. Present-day atmospheric simulations using GISS ModelE: Comparison to in situ, satellite, and reanalysis data. J. Clim., 19(2), 153-192.

Scoccimarro, E., Gualdi, S., Bellucci, A., Sanna, A., Giuseppe Fogli, P., Manzini, E., Vichi, M., Oddo, P. and Navarra, A., 2011. Effects of tropical cyclones on ocean heat transport in a high-resolution coupled general circulation model. J. Clim., 24(16), 4368-4384.

Tjiputra, J.F., Roelandt, C., Bentsen, M., Lawrence, D.M., Lorentzen, T., Schwinger, J., Seland, Ø. and Heinze, C., 2013. Evaluation of the carbon cycle components in the Norwegian Earth System Model (NorESM). Geosci. Model Dev., 6(2), 301-325.

Voldoire, A., Sanchez-Gomez, E., y Mélia, D.S., Decharme, B., Cassou, C., Sénési, S., Valcke, S., Beau, I., Alias, A., Chevallier, M. and Déqué, M., 2013. The CNRM-CM5. 1 global climate model: description and basic evaluation. Clim. Dyn., 40(9-10), 2091-2121.

Volodin, E.M., Dianskii, N.A. and Gusev, A.V., 2010. Simulating present-day climate with the INMCM4. 0 coupled model
of the atmospheric and oceanic general circulations. Izv. Atmos. Ocean. Phys., 46(4), 414-431.

Watanabe, S., Hajima, T., Sudo, K., Nagashima, T., Takemura, T., Okajima, H., Nozawa, T., Kawase, H., Abe, M., Yokohata, T. and Ise, T., 2011. MIROC-ESM 2010: Model description and basic results of CMIP5-20c3m experiments. Geosci. Model Dev., 4(4), 845.

Wu, T., 2012. A mass-flux cumulus parameterization scheme for large-scale models: Description and test with observations.
Clim. Dyn., 38(3-4), 725-744.

Yukimoto, S., Adachi, Y., Hosaka, M., Sakami, T., Yoshimura, H., Hirabara, M., Tanaka, T.Y., Shindo, E., Tsujino, H., Deushi, M. and Mizuta, R., 2012. A new global climate model of the meteorological research institute: MRI-CGCM3-Model description and basic performance. J. Meteor. Soc. Jpn., 90, 23-64.